Large Exploration by Small Payloads: Underwater Deployables via Robot Swarms

Pascal Spino[1,2], Marc Bäckert[1], Lianhao Yin[1], and Daniela Rus[1]

***Abstract*— This paper presents a swarm-deployable approach for ocean-world exploration, where centimeter-scale underwater robots self-assemble into chain aggregates to improve swimming performance. Physical experiments with up to eight 6 cm-scale robots show that aggregation can nearly double swim speed or reduce cost of transport by almost an order of magnitude, enabling small payloads to dynamically reconfigure into more capable underwater systems. More broadly, this architecture has deployable-like properties that may extend beyond locomotion to shared sensing and computation, effectively building larger and more capable robotic systems from many smaller, simpler robots.**

I. INTRODUCTION

The vast subsurface oceans of Europa, Enceladus, and as many as ten other ocean worlds within our solar system are among the least-understood and most compelling environments for future robotic space exploration [1]. However, any system that would explore these environments is subject to severe size and mass constraints due to the physics of ocean access on these ice-covered bodies; emerging architectures for thermomechanical ice drilling units support payload volumes less than 20 L in even the most optimistic mission architectures [2]. Europa, among the highest priority targets of the ocean moons, may have an ocean volume more than twice as large as all the oceans of Earth combined at $\sim 3 \times 10^{21}$ L [3]. A central challenge, then, is how to design such small payloads that can meaningfully traverse and explore such vast underwater regions. Prior work has identified miniaturized swarm architectures as a promising approach [2], enabling spatially distributed sensing and robustness to individual failures. However, the endurance and range of these vehicles remain fundamentally limited by physics: smaller swimmers are slower and less energetically efficient than larger swimmers [4]. This work investigates a deployable-like approach to improve the swimming performance of swarms of small underwater vehicles. We develop a 100 mL-class autonomous underwater robot that can magnetically connect and coordinate propulsion with other units, enabling substantial gains in both swim speed and efficiency. A chain aggregate of eight robots demonstrates nearly an order of magnitude improvement in endurance and approximately a twofold increase in swim speed relative to a single unit, approaching velocities of 1 knot or a cost of transport as low as 2 for a $\sim$1 L-scale payload. The robot swarm can dynamically alter its capabilities through in-situ self-assembly and coordinated actuation. For example, robots may aggregate to traverse long distances or overcome strong currents, and subsequently disperse to distribute sensing across a larger area. In this way the swarm architecture demonstrates the properties of a spacecraft deployable [5]. Traditional deployables, such as antennas or solar arrays, are compact during launch and expand in situ to achieve functionality that would otherwise exceed payload constraints. The swarm architecture presented here extends this concept to mobile robotic systems; instead of deploying a single robot, the system deploys many independent robotic units that can physically assemble into larger functional morphologies.

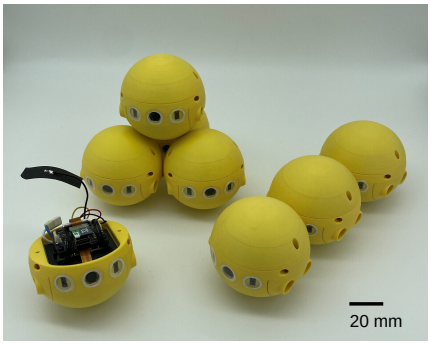

Fig. 1. A fleet of eight BμBL robots used in this work. Individual robots can connect by magnetic couplings to form chains or other topologies.

II. SYSTEM OVERVIEW

The robotic platform used in this work is an experimental underwater vehicle, termed BμBL, designed for autonomous operation and multi-agent aggregation [6], [7]. Each robot measures 64 mm in diameter, has a mass of 127 g, and carries its own onboard battery, sensing, computation, and propulsion systems. Autonomous operation can be sustained for 30 mins on a single battery charge. The platform is capable of wireless communication via Bluetooth Low Energy (BLE) when near the surface and otherwise operates autonomously, logging all sensor and control data at 50 Hz to onboard storage. Locomotion is achieved using four independently controlled fluid jet propulsors arranged symmetrically around the equator of the robot. Each propulsor draws water through an inlet and expels it through a narrow outlet, producing thrust proportional to motor speed. In static tests, individual jets generate up to 75 mN of thrust. By coordinating the four jets, the robot produces body forces and torques for control of forward motion, depth, and full attitude (roll,

[1]Computer Science and Artificial Intelligence Laboratory, Massachusetts Institute of Technology, Cambridge, MA, 02139, USA

[2]Department of Mechanical Engineering, Massachusetts Institute of Technology, Cambridge, MA, 02139, USA spino@mit.edu

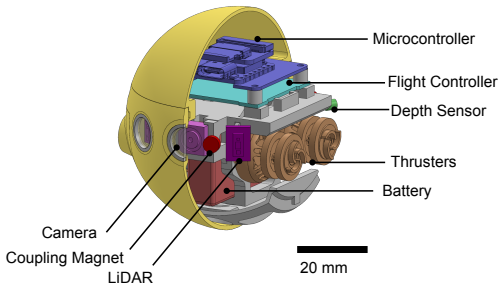

Fig. 2. Diagram of the BμBL robot with a cross section of the watertight shell. Each robot is equipped with four water jet propulsors and packed with a small suite of sensors and processors.

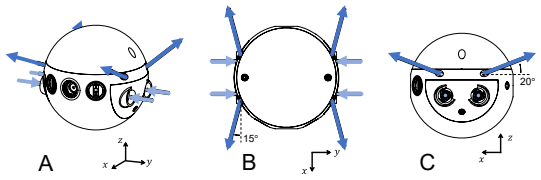

Fig. 3. Schematic of the BμBL propulsion system. The robot is equipped with four mirrored propulsors that resemble centrifugal pumps. Each propulsor intakes water from an inlet on the side of the vehicle (light blue) and expels it from a jet near the equator (dark blue); each jet is precisely angled 20° above the equatorial plane, and 15° to the side. The robot is controlled by regulating the flow rate of each jet. (A) isometric view. (B) top-down view, with the robot facing downwards. (C) side-view, with the robot facing left.

pitch, and yaw). The jet outlets are angled to reduce hydrodynamic interference between neighboring robots, enabling efficient operation in multi-robot chain aggregates. To support autonomous behavior, each robot is equipped with a lightweight sensing suite including a forward-facing camera, two multizone LiDAR sensors, a six-axis IMU, and a pressure sensor. While the LiDAR sensors provide short-range obstacle detection ($\sim$16 cm underwater), the camera enables perception at meter-scale distances. A low-compute onboard vision algorithm performs color-based blob detection at up to 90 Hz, extracting target bearing and approximate range from image features to enable visual servoing and relative positioning. A key feature of the platform is a passive magnetic docking mechanism that enables physical connection between robots. Each robot includes front and rear docking interfaces composed of paired neodymium magnets arranged to enforce alignment. For separations below 9 mm and angular mismatch below 20°, robots passively self-align and dock. The interface supports tensile loads up to 350 mN, allowing connected robots to transmit propulsion forces and form stable chain aggregates. Undocking is achieved through coordinated actuation of the propulsion system to generate separating torques between robots. Through this combination of compact actuation, onboard sensing, and passive mechanical coupling, the system enables groups of robots to dynamically assemble into larger structures.

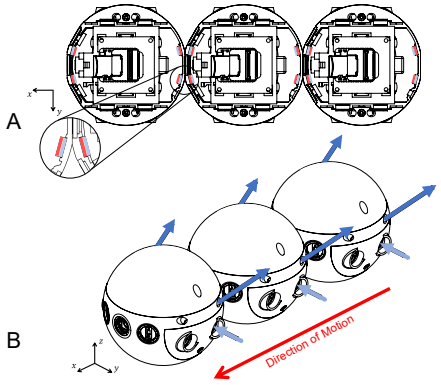

Fig. 4. (A) Top-down view of a chain of three docked robots, with cross-section of the shell to show the arrangement of internal docking magnets (colored red and blue to indicate polarity) (B) Isometric view of a chain of three docked robots showing the vectors of fluid jets from each robot and the resulting aggregate direction of motion.

III. Experimental Results

Experiments evaluate how physical aggregation of robots affects swim speed and efficiency of the collective. Robots are tested both individually and in linear chain aggregates of up to eight units. Tests were performed in a $4\,\mathrm{m} \times 3\,\mathrm{m} \times 1\,\mathrm{m}$ fresh water pool with each robot logging its power consumption by onboard sensing, and an overhead camera providing footage to extract speed measurements. Two chain aggregate propulsion strategies are considered: (i) *all-thrust*, where each robot contributes equally to propulsion, and (ii) *rear-thrust*, where only the trailing robot produces thrust while the remaining robots are passive. Aggregate performance is measured in terms of steady-state swim speed and cost of transport (CoT), defined as the electrical power consumed per unit weight and velocity (Eq.1). Across all experiments, individual robots operate at approximately constant electrical power for a given throttle input. In the all-thrust configuration, aggregate speed increases monotonically with chain length. An eight-robot chain achieves velocities of $41\,\mathrm{cm/s}$, representing roughly a twofold increase over a single robot under comparable operating conditions. In contrast, the rear-thrust configuration demonstrates substantial improvements in energetic efficiency. For the largest aggregates tested, CoT decreases by nearly an order of magnitude relative to a single robot, reaching values as low as 2.

$$\mathrm{CoT} = \frac{\sum_{i=1}^{N} P_i}{N\, m\, g\, v} \tag{1}$$

These results highlight a tradeoff between speed and efficiency that can be modulated through the coordination of each robot's propulsion. All-thrust aggregates maximize traversal speed, while rear-thrust aggregates minimize energy expenditure. Figure 5 visualizes the results of all experiments.

IV. Discussion

This work explored modular architectures for centimeter-scale underwater robots using magnetically docking units

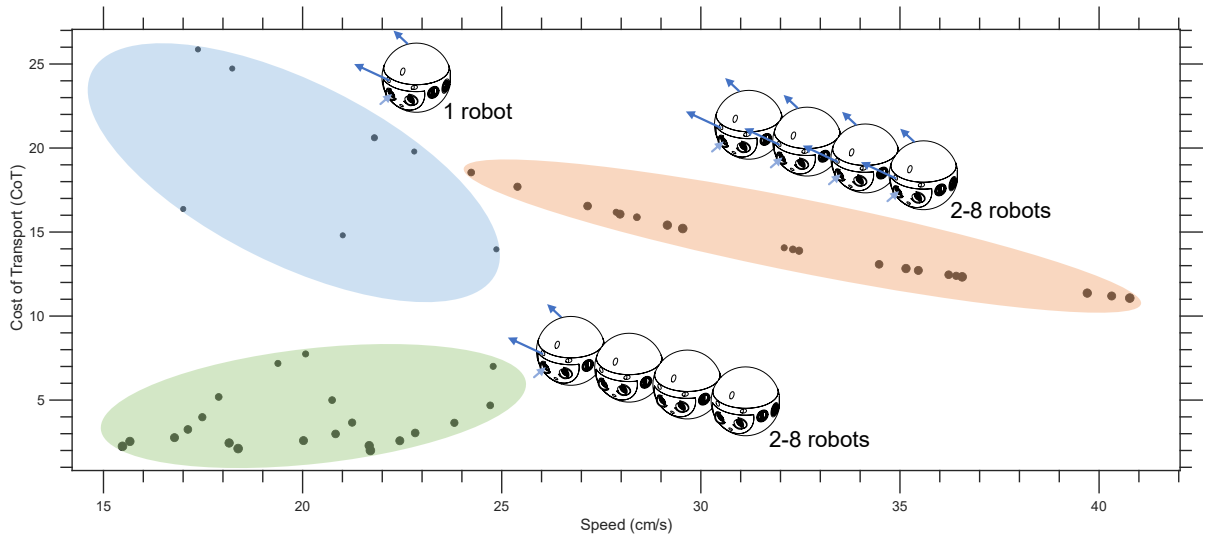

Fig. 5. CoT–speed plot summarizing all aggregate chain propulsion experiments. Each point represents a configuration for which steady swimming speed and electrical power were experimentally measured, and cost of transport (CoT) was computed from these measurements using Equation 1. Point size indicates the number of robots in the chain, with larger points corresponding to larger aggregates. Ellipses highlight three distinct clusters that emerge in the data. The upper-left blue cluster corresponds primarily to single-robot configurations (with one two-robot configuration), the lower-left green cluster corresponds to rear-only thrust chains with two or more robots, and the upper-right red cluster corresponds to all-thrust chains with two or more robots. The separation of these clusters illustrates how different propulsion strategies occupy distinct regions of the CoT–speed space. In particular, multi-robot aggregates reach performance regimes unavailable to a single robot, achieving substantially higher swimming speeds and lower cost of transport.

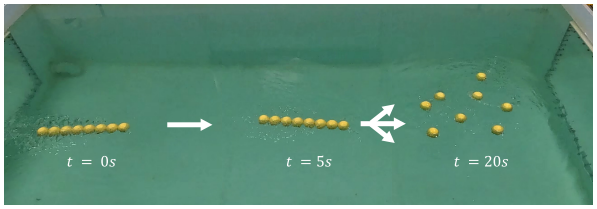

Fig. 6. A chain of eight BμBL robots traverses half of the tank as a chain aggregate and then self-disassembles into individual robots.

capable of autonomous self-assembly and disassembly. The robots behave as a deployable by combining to build a larger, more capable robotic structure. The combined structure exhibits a reduced frontal surface area relative to independent swimmers, resulting in lower drag. Experiments show that chain aggregates outperform individual robots in both speed and cost of transport (CoT). When all robots apply thrust, chain aggregates achieve substantially higher speeds, reaching up to $41\,\mathrm{cm/s}$ in the eight-robot case—nearly an 80% increase over a single robot. In contrast, when only the rear robot provides thrust, locomotion efficiency improves dramatically, reducing CoT from 14–16 to approximately 2. These results highlight a tradeoff between speed and efficiency that can be modulated through collective propulsion strategy. By exploiting reversible self-assembly, robot swarms can dynamically adjust their capabilities to match the task at hand. For example, robots may form aggregates to traverse long distances efficiently or generate higher thrust to overcome strong currents, and subsequently disperse to increase spatial coverage during sensing or exploration (Figure 6) In this work, only two extreme propulsion strategies were examined—uniform thrust and rear-only thrust—but a wide space of intermediate control strategies exists in which thrust is distributed non-uniformly across the aggregate. Exploring these regimes may reveal additional tradeoffs between speed and efficiency.

Several directions for future work follow from these results. Improved understanding of fluid interactions among distributed propulsors may inform more effective coordination strategies. In the present experiments, each robot operated using local proportional-derivative control with no explicit coordination beyond mechanical coupling, which limits overall system performance. Future approaches may instead leverage shared sensing across the aggregate and coordinated control of propulsion to more fully exploit the capabilities of the collective system. More broadly, an open question is how sensing, computation, and actuation can be synthesized across physically connected swarms under minimal communication constraints, enabling the aggregate to function as a single coordinated robotic system. This area of work extends to other types of spacecraft deployables that may benefit from modular self-assembling swarm architectures, such as reconfigurable satellite clusters or cooperative rovers. Finally, future work should explore how this underwater swarm-deployable strategy may be applied with field-deployable robots in real world environments.

ACKNOWLEDGMENT

Pascal Spino is supported by a NASA Space Technology Graduate Research Opportunities Fellowship (NSTGRO) under grant number 80NSSC25K0239. The authors acknowledge the SMART M3 program and ONR Science of Autonomy under grant number N00014-23-1-2354.

REFERENCES

[1] A. R. Hendrix, T. A. Hurford, L. M. Barge, M. T. Bland, J. S. Bowman, W. Brinckerhoff, B. J. Buratti, M. L. Cable, J. Castillo-Rogez, G. C. Collins, S. Diniega, C. R. German, A. G. Hayes, T. Hoehler, S. Hosseini, C. J. Howett, A. S. McEwen, C. D. Neish, M. Neveu, T. A. Nordheim, G. W. Patterson, D. A. Patthoff, C. Phillips, A. Rhoden, B. E. Schmidt, K. N. Singer, J. M. Soderblom, and S. D. Vance, "The nasa roadmap to ocean worlds," *Astrobiology*, vol. 19, no. 1, pp. 1–27, 2019, pMID: 30346215. [Online]. Available: https://doi.org/10.1089/ast.2018.1955

[2] E. W. Schaler, M. Reinders, M. Holst, H. J. Lee, M. Samnani, T. Schafer, J. Holland, K. Bhingradiya, B. Liang, J. Vizcarra, J. Izraelevitz, S. Howell, E. Lesage, Z. Hao, and A. Ansari, "Design and development of swim – miniature, untethered underwater robots for exploring ice-ocean interfaces," in *2024 IEEE Aerospace Conference*, vol. 1. IEEE, Mar. 2024, p. 1–20. [Online]. Available: http://dx.doi.org/10.1109/AERO58975.2024.10521345

[3] J. D. Anderson, G. Schubert, R. A. Jacobson, E. L. Lau, W. B. Moore, and W. L. Sjogren, "Europa's differentiated internal structure: Inferences from four galileo encounters," *Science*, vol. 281, no. 5385, p. 2019–2022, Sep. 1998. [Online]. Available: http://dx.doi.org/10.1126/science.281.5385.2019

[4] A. B. Phillips, M. Haroutunian, S. K. Man, A. J. Murphy, S. W. Boyd, J. I. Blake, and G. Griffiths, *Nature in engineering for monitoring the oceans: comparison of the energetic costs of marine animals and AUVs*. Institution of Engineering and Technology, Jan. 2012, p. 373–405. [Online]. Available: http://dx.doi.org/10.1049/PBCE077E_ch17

[5] B. Wang, J. Zhu, S. Zhong, W. Liang, and C. Guan, "Space deployable mechanics: A review of structures and smart driving," *Materials amp; Design*, vol. 237, p. 112557, Jan. 2024. [Online]. Available: http://dx.doi.org/10.1016/j.matdes.2023.112557

[6] P. Spino and D. Rus, "Towards centimeter-scale underwater mobile robots: An architecture for capable μauvs," in *2024 IEEE International Conference on Robotics and Automation (ICRA)*. IEEE, May 2024, p. 1484–1490. [Online]. Available: http://dx.doi.org/10.1109/ICRA57147.2024.10610474

[7] ——, "Bμbl: A centimeter-scale underwater robot," in *International Symposium on Experimental Robotics (ISER)*, 2025, to appear.